ORIGINAL ARTICLE

Preclinical evaluation of [99mTc]Tc-labeled anti-EpCAM nanobody for EpCAM receptor expression imaging by immuno-SPECT/CT

Tianyu Liu[1] · Yue Wu[1] · Linqing Shi[1] · Liqiang Li[1] · Biao Hu[1] · Yanpu Wang[1] · Hannan Gao[1] · Xiaolu Yu[2] · Xin Zhang[1] · Huiyun Zhao[1] · Yakun Wan[3] · Bing Jia[1,4] · Fan Wang[1,5]

Abstract

Purpose Overexpression of epithelial cell adhesion molecule (EpCAM) plays essential roles in tumorigenesis and tumor progression in almost all epithelium-derived cancer. Monitoring EpCAM expression in tumors can be used for the diagnosis, staging, and prognosis of cancer patients, as well as guiding the individualized treatment of EpCAM-targeted drugs. In this study, we described the synthesis and evaluation of a site-specifically [99mTc]Tc-labeled EpCAM-targeted nanobody for the SPECT/CT imaging of EpCAM expression.

Methods We first prepared the [99mTc]Tc-HYNIC-G_4K; then, it was site-specifically connected to EpCAM-targeted nanobody NB4. The in vitro characteristics of [99mTc]Tc-NB4 were investigated in HT-29 (EpCAM positive) and HL-60 (EpCAM negative) cells, while the in vivo studies were performed using small-animal SPECT/CT in the subcutaneous tumor models and the lymph node metastasis model to verify the specific targeting capacity as well as the potential applications of [99mTc]Tc-NB4.

Results [99mTc]Tc-NB4 displayed a high EpCAM specificity both in vitro and in vivo. SPECT/CT imaging revealed that [99mTc]Tc-NB4 was cleared rapidly from the blood and normal organs except for the kidneys, and HT-29 tumors were clearly visualized in contrast with HL-60 tumors. The uptake value of [99mTc]Tc-NB4 in HT-29 tumors was increased continuously from $3.77 \pm 0.39\%ID/g$ at 0.5 h to $5.53 \pm 0.82\%ID/g$ at 12 h after injection. Moreover, the [99mTc]Tc-NB4 SPECT/CT could clearly image tumor-draining lymph nodes.

Conclusion [99mTc]Tc-NB4 is a broad-spectrum, specific, and sensitive SPECT radiotracer for the noninvasive imaging of EpCAM expression in the epithelium-derived cancer and revealed a great potential for the clinical translation.

Keywords Immuno-SPECT/CT · EpCAM imaging · [99mTc]Tc-Nanobody · Site-specific radiolabeling

Introduction

Epithelial cell adhesion molecule (EpCAM) is a type I transmembrane glycoprotein which mediates Ca^{2+}-independent homotypic cell adhesion, acting as an important cancer biomarker [1, 2]. The high expression of EpCAM has been

✉ Bing Jia
jiabing@bjmu.edu.cn

✉ Fan Wang
wangfan@bjmu.edu.cn

1 Medical Isotopes Research Center, Department of Radiation Medicine, School of Basic Medical Sciences, Peking University, Beijing 100191, People's Republic of China

2 State Key Laboratory of Drug Research, Shanghai Institute of Materia Medica, Chinese Academy of Sciences, Shanghai 201203, People's Republic of China

3 Shanghai Novamab Biopharmaceuticals Co., Ltd, Shanghai, People's Republic of China

4 Department of Integration of Chinese and Western Medicine, School of Basic Medical Sciences, Peking University, Beijing 100191, People's Republic of China

5 Key Laboratory of Protein and Peptide Pharmaceuticals, CAS Center for Excellence in Biomacromolecules, Institute of Biophysics, Chinese Academy of Sciences, Beijing 100101, People's Republic of China

found on a great variety of human adenocarcinomas and squamous cell carcinomas like breast, lung, colon, renal, gastric, prostate, and ovarian cancer [3, 4]. Its expression level in cancer correlates well with tumor progression and invasiveness of almost all epithelium-derived tumors. Overexpression of EpCAM in some tumors such as breast cancer, hepatocellular cancer, pancreatic cancer, and ovarian cancer indicates poor therapeutic outcomes and prognosis [1, 5, 6]. Consequently, EpCAM is an ideal therapeutic target for the treatment of the most frequent EpCAM-positive human cancers. Monoclonal antibodies against EpCAM have been developed, from the earliest therapeutic antibody edrecolomab for gastrointestinal adenocarcinoma to the trifunctional, bispecific antibody catumaxomab that has been approved for clinical use today [7–9]. However, not all patients have good responses to these drugs, which may be related to the EpCAM expression level or heterogeneity of the tumor itself. We are unable to perform a biopsy on each tumor, so the noninvasive assessment methods of EpCAM expression are essential, which is of great significance for the diagnosis and prognosis of tumors, as well as guiding the subsequent treatment.

Molecular imaging can noninvasively detect dynamic molecular processes in normal or pathological conditions in vivo, offering unlimited possibilities for accurate diagnosis and sensitive tumor detection [10]. Accordingly, molecular imaging agents that target EpCAM would be highly useful in the detection of epithelium-derived tumors. Recent studies have been successfully performed on the development of radiotracers for in vivo EpCAM imaging, such as antibodies [11–13]. Variable heavy chain domain of heavy-chain-only antibodies (VHH), also known as nanobody, was derived from heavy-chain-only antibodies which were found naturally in Camelidae [14]. Nanobody has a small molecular weight of 15 kDa, so it has a better penetration of tissue, a rapid diffusion and a faster biodistribution [15]. Compared to the current EpCAM-targeted antibody molecular probes, the nanobody-based molecular probes have better tissue permeability and faster body clearance. Meanwhile, owing to the moderate radioactivity half-life period of 6.02 h, ^{99m}Tc is well suited for capturing the in vivo pharmacokinetics of nanobodies. In order to ensure the high activity and high stability of the radiotracer, site-specific radiolabeling is a pretty good strategy for proteins. Sortases are bacterial transpeptidases that are used for efficient protein engineering [16–18]. Herein, we chose a G_4K short peptide (sequence: GGGGK) for the sortase A-mediated site-specific modification of the EpCAM-targeted nanobody, then prepared a [^{99m}Tc]Tc-labeled nanobody to image tumors in the subcutaneous tumor models and the tumor lymph node metastasis model by immuno-SPECT/CT, and compared with [^{18}F]FDG PET/CT imaging to investigate its EpCAM targeting capability.

Materials and methods

Preparation of [^{99m}Tc]Tc-NB4

The LPETG-His$_6$ modified EpCAM-targeted nanobody (NB4) was provided by Prof. Yakun Wan (Shanghai Institute of Materia Medica, Shanghai, China). Chemicals and solvents were purchased from *Sigma-Aldrich* (St. Louis, MO, USA). The synthesis process of GGGGK-HYNIC (shorted as HYNIC-G$_4$K) is shown in the supplementary information. HYNIC-G$_4$K was labeled with ^{99m}Tc using N-tris-hydroxymethyl-methylglycine (Tricine) and trisodium triphenylphosphine-3,3',"-trisulfonate (TPPTS) as the co-ligands [19] to obtain [^{99m}Tc]Tc-HYNIC-G$_4$K. HYNIC-G$_4$K (0.01 μmol) was mixed with combined solutions of 5 mg of tricine and 5 mg of TPPTS (in 150 μL of 50 mM succinate buffer, pH 4.9). [^{99m}Tc]NaTcO$_4$ (370 MBq) was then added to the solution and stirred at 100 °C for 20 min. The radiochemical purity of [^{99m}Tc]Tc-HYNIC-G$_4$K was determined by radio-HPLC. Five hundred microliter reaction mixtures contained 50 mM Tris–HCl, 10 mM CaCl$_2$, 100 mM NaCl, 200 μM [^{99m}Tc]Tc-HYNIC-G$_4$K, 200 μM NB4, and 50 μM sortase A. The pH of the mixture was adjusted to 7.5 and the mixture was stirred for 20 min at 37 °C [17, 18]. The radiochemical purity of [^{99m}Tc]Tc-NB4 was determined by Instant Thin Layer Chromatography Medium (iTLC, AR-2000 (Bioscan, USA)). Then, the mixture was purified by size-exclusion chromatography HPLC using Superose 12 (GE LifeScience, Pittsburgh, USA). The radiochemical purity of [^{99m}Tc]Tc-NB4 was higher than 97% after purification.

Cell and animal models

The HT-29 human colorectal adenocarcinoma cell line was purchased from American Type Culture Collection (Manassas, VA, USA). The HL-60 human acute promyelocytic leukemia cell line was provided by Prof. Xiaoyan Qiu (NHC Key Laboratory of Medical Immunology, Peking University). Cells were maintained under standard conditions according to ATCC. Firefly luciferase stably transfected HT-29-Luc cells were generated as described in the supplemental materials and methods. The HT-29 cells and HT-29-Luc cells grew in DMEM/F12 medium supplemented with 5% fetal bovine serum (FBS). The HL-60 cells grew in RPMI-1640 medium supplemented with 10% FBS. Both cancer cell lines were cultured at 37 °C in a humidified atmosphere containing 5% CO$_2$.

Animal housing and welfare conditions are described in the supplementary information. BALB/c nude mice (4 weeks of age) were obtained from the Department of Laboratory Animal Science of Peking University. To establish HT-29

subcutaneous tumor models, 5×10^6 HT-29 cells were inoculated subcutaneously into the right front flanks of female BALB/c nude mice. For the HT-29/HL-60 bilateral tumor model, 5×10^6 HL-60 cells (in 100 µL of PBS, which was mixed with 50% Matrigel (Corning, NY, USA)) were subcutaneously inoculated into the left front flanks of female BALB/c nude mice. After that, 5×10^6 HT-29 cells were subcutaneously inoculated into the right front flanks of the same female BALB/c nude mice 6 days later. The animals were used for in vivo studies when the tumor size reached 200–300 mm^3 (2–3 weeks after inoculation).

For the lymph node metastasis model, 2×10^5 HT-29-Luc cells were injected into the left front and hind footpads of female BALB/c mice. The growth of lymph node metastatic tumors was monitored by bioluminescence imaging (BLI) as previously described [20]. Every 7 days, we used BLI to detect lymph node metastasis, and during each BLI, we used black tape to completely cover the tumors in the footpad to reduce in situ autofluorescence interference. Animal models were used for in vivo studies when tumor lymph node metastasis was detected on day 21. The average BLI signal of axillary and popliteal lymph nodes were 1.62 ± 0.57 and 1.22 ± 0.32 (unit: $\times 10^5$ p/s/cm^2/sr).

Binding of NB4 to EpCAM

To verify the cross-species of EpCAM-targeted NB4, human, rhesus, and mouse EpCAM proteins were used to bind with NB4. [125I]I-NB4 was prepared by labeling NB4 with [125I]NaI using the Iodogen method, as previously described [21]. [125I]I-NB4 (3.0 kBq) was added to 96-well Stripwell™ enzyme-linked immunosorbent assay (ELISA) plates (Costar, Cambridge, MA) coated with 0.2 µg human, rhesus, or mouse EpCAM protein per well with or without an excess dose of cold NB4 (4 µg/well). After incubation for 1 h at 37 °C, the plates were washed with ice-cold PBS containing 0.05% Tween-20 (PBST) to remove free radioactivity, and wells were collected and measured in a calibrated γ-counter (Wallac 1470–002, Perkin Elmer, Finland). All experiments were performed twice with four samples for each. Results were expressed as CPM per 1 pmol protein.

To evaluate the expression status of EpCAM in HT-29 and HL-60 cells, immunofluorescence staining and flow cytometry experiments were carried out. For immunofluorescence staining, approximately 1×10^5 HT-29/HL-60 cells were seeded into confocal dishes. Cells were incubated with NB4 as primary antibodies for 2 h at room temperature after blocking with 5% FBS in PBS, followed by incubation with Anti-6X His tag antibody with DyLight 650 (Abcam, Cambridge, UK) as a secondary antibody for 1 h at room temperature and visualized using a confocal microscope (Wetzler, Heidelberg, Germany). Flow cytometry analysis of EpCAM expression levels in HT-29 and HL-60 cells is described in the supplementary information.

In order to identify the binding level of NB4 to EpCAM-positive HT-29 cells and EpCAM-negative HL-60 cells at the cellular level, we conducted cell-binding experiments. [99mTc]Tc-NB4 was prepared as mentioned above. HT-29 and HL-60 tumor cells were trypsinized to obtain single-cell suspensions and were transferred to the Eppendorf tube (2×10^6 cells in 200 µL of PBS with 1% BSA per tube). [99mTc]Tc-NB4 (7.4 kBq) was added to each tube with or without an excess dose of cold NB4 (1000-folds excess) for 2 h at 4 °C. The cells were washed with ice-cold PBST soon afterward to remove free radioactivity. Then, the cells with bound radioactivity were collected, and the radioactivity was measured in a calibrated γ-counter. All experiments were performed twice with four samples for each. Results were expressed as CPM per 10^6 cells. [99mTc]Tc-NB4 cell internalization experiments are described in the supplementary information.

Small-animal PET/CT and SPECT/CT imaging

The small-animal SPECT/CT imaging was performed on BALB/c nude mice bearing HT-29 cancer xenografts and HT-29/HL-60 bilateral cancer xenografts. Mice were allowed to wake up after probe injection. The pinhole SPECT images (peak: 140 keV, 20% width; frame time: 30 s) were acquired for 27 min, and subsequently, CT images were acquired (50 kVp, 0.67 mA, rotation 210°, exposure time: 300 ms). All SPECT images were reconstructed and further analyzed with Fusion (Mediso, Budapest, Hungary) [22].

For the HT-29 tumor model, each tumor-bearing nude mouse was injected via the tail vein with 18 MBq of [99mTc]Tc-NB4. At 30 min, 1 h, 2 h, 4 h, 8 h, and 12 h post-injection (p.i.), the mice were anesthetized by inhalation of 2% isoflurane and imaged using nanoScan following a standard protocol. For the HT-29/HL-60 bilateral tumor model, each tumor-bearing nude mouse was injected via the tail vein with 18 MBq of [99mTc]Tc-NB4. At 30 min, 1 h, 2 h p.i., the mice were imaged using the same method using nanoScan.

The small-animal PET/CT imaging was performed on BALB/c nude mice bearing HT-29/HL-60 bilateral cancer xenografts. Each tumor-bearing nude mouse was injected via the tail vein with 18 MBq of [18F]FDG. Mice were kept unconscious under 2% isoflurane for 60 min p.i. to prevent tracer uptake in muscles. The body temperature of unconscious mice was maintained by a controllable electric blanket. At 1 h p.i., the mice were imaged using nanoScan (Mediso, Budapest, Hungary) following a standard protocol.

For the imaging of the lymph node metastasis model, each HT-29-Luc tumor-bearing BALB/c nude mouse was injected via the tail vein with 18 MBq of [^{99m}Tc]Tc-NB4. SPECT images were acquired at 3 h p.i. using nanoScan. In order to determine the probe aggregation of the tumor-draining lymph nodes, 10 μL 1% Evans Blue was injected into each paw pad, and the mice were sacrificed after 3 min p.i. The bilateral axillary lymph nodes and popliteal lymph nodes of the mice that were stained blue by Evans Blue were removed and placed next to the mice to re-execute SPECT/CT imaging.

Biodistribution of [^{99m}Tc]Tc-NB4

For HT-29 tumor model's ex vivo biodistribution, female nude mice bearing HT-29 tumor xenografts were injected by tail vein with 0.37 MBq of [^{99m}Tc]Tc-NB4 to evaluate the distribution of [^{99m}Tc]Tc-NB4 in major organs and tumors ($n = 4$ per group). Meanwhile, cold NB4 was calculated and co-injected to ensure that the doses of SPECT/CT imaging and biodistribution were consistent. The mice were sacrificed and dissected at 30 min, 1 h, 2 h, 4 h, 8 h, and 12 h p.i., and tumor, kidney, blood, and other major organs were collected and weighted. Samples and prime standards were counted for radioactivity in a calibrated γ-counter. The ex vivo tissue activity is presented as the percentage of injection dose per gram of tissue (%ID/g). The blocking study was also performed in HT-29 mice by a co-injection of 0.37 MBq of [^{99m}Tc]Tc-NB4 with an excess dose of cold NB4 (1 mg). At 2 h p.i., the blocked mice were sacrificed and dissected. Then, the organ biodistribution of [^{99m}Tc]Tc-NB4 was determined.

For HT-29/HL-60 bilateral tumor model's ex vivo biodistribution, mice bearing HT-29/HL-60 bilateral tumor xenografts were injected with 0.37 MBq of [^{99m}Tc]Tc-NB4 to evaluate the distribution of [^{99m}Tc]Tc-NB4 in major organs and tumors ($n = 4$ per group). Subsequently, organs and tissues were excised and weighed at 2 h p.i. Samples and prime standards were counted for radioactivity in a calibrated γ-counter. The ex vivo tissue activity is also presented as %ID/g.

Statistical analysis

Quantitative data are expressed as the mean $\pm$ SD. We used the Shapiro–Wilk test to detect the normality of each set of data including binding experiments and biodistribution that requires statistical analysis. If $P > 0.05$, it was considered to pass the normality test. After testing, it was found that the data for each group of statistical analysis were in accordance with the normal distribution. Statistical analysis was then performed with a two-tailed Student's t-test with Welch's correction with GraphPad Prism 8.0 (GraphPad Software, Inc.). $P < 0.05$ was considered statistically significant.

Fig. 1 **a**, **b** Structure of GGGGK-HYNIC and [^{99m}Tc]Tc-NB4. **c** Synthetic route of [^{99m}Tc]Tc-NB4
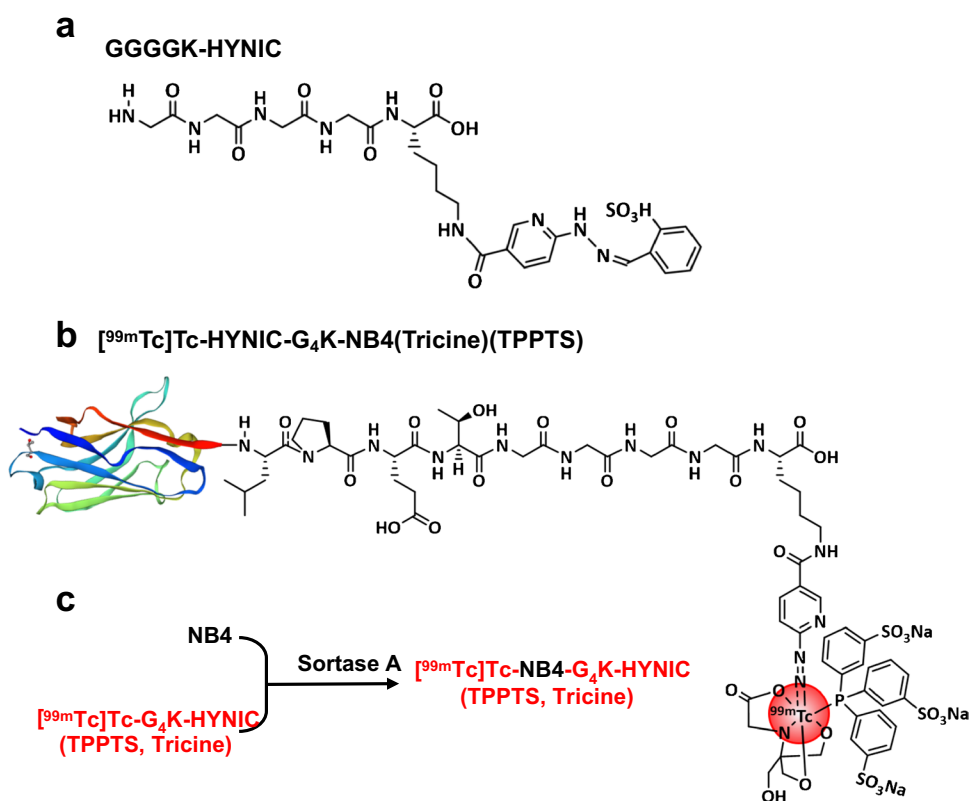
Results

Chemistry and radiochemistry

HYNIC-G_4K (Fig. 1a) was obtained in a 43.3% yield and was confirmed by mass spectroscopy analysis. Matrix-assisted laser desorption/ionization time-of-flight mass spectrometry detected 678.2 (m/z) ($C_{27}H_{35}N_9O_{10}S$, exact mass: 677.22) (Fig. S1a). The [^{99m}Tc]Tc-labeling procedure of HYNIC-G_4K was done within 20 min, and the radiochemical purity of [^{99m}Tc]Tc-HYNIC-G_4K was greater than 98% as determined by radio-HPLC (Fig. S1b). The tailing peak for [^{99m}Tc]Tc-HYNIC-G_4K is discussed in supplementary data. The preparation of [^{99m}Tc]Tc-labeled EpCAM-targeted NB4 nanobody, [^{99m}Tc]Tc-HYNIC-G_4K-NB4(Tricine) (TPPTS) (shorted as [^{99m}Tc]Tc-NB4), was also done within 20 min. Using physiological saline as a developing agent, the radiolabeling yield determined by iTLC was about 60% (Fig. S2a). After the purification of Superose 12, the radiochemical purity of [^{99m}Tc]Tc-NB4 was greater than 97% as

determined by iTLC (Fig. S2b). The structure of [^{99m}Tc]Tc-NB4 is shown in Fig. 1b. The synthetic route for [^{99m}Tc]Tc-NB4 is shown in Fig. 1c.

In vitro verification of EpCAM-targeted specificity of NB4

We first validated by flow cytometry that HT-29 cells highly expressed EpCAM, and HL-60 was EpCAM negative (Fig. S2c), consistent with previous experimental studies [13]. Protein binding experiments showed that NB4 was highly selective for EpCAM proteins of different species (Fig. 2a). NB4 bound almost exclusively to the human EpCAM protein, while having little binding to murine and rhesus EpCAM proteins (1255.59 ± 25.11 vs. 14.89 ± 3.02; $P < 0.0001$, and 1255.59 ± 25.11 vs. 19.19 ± 7.25; $P < 0.0001$). The excessive cold NB4 could significantly inhibit the binding of [^{125}I]I-NB4 to human EpCAM (from 1255.59 ± 25.11 to 66.75 ± 7.97; $P < 0.0001$). In cell-binding assays, the binding value (CPM per 10^6 cells) of [^{99m}Tc]Tc-NB4 to HT-29 cells was


Fig. 2 **a** Protein binding of [^{125}I]I-NB4 to human, rhesus, and mouse EpCAM. ****, $P < 0.0001$. **b** Cell binding of [^{99m}Tc]Tc-NB4 to HT-29 (EpCAM positive) and HL-60 (EpCAM negative) tumor cells. **, $P < 0.01$. **c** EpCAM immunofluorescence staining in HT-29 and HL-60 tumor cells with NB4 as the primary antibody and anti-His tag antibody with DyLight as the secondary antibody
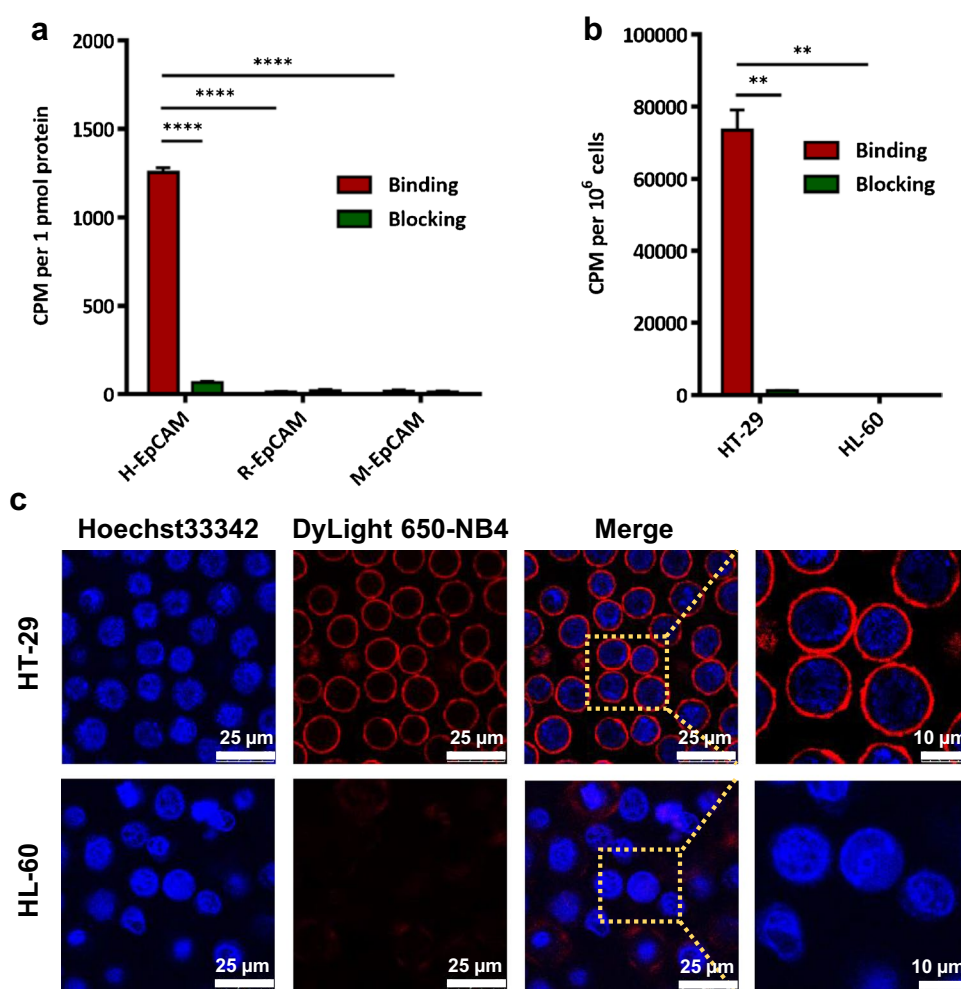
much higher than that to HL-60 cells ($73{,}412.20 \pm 5689.99$ vs. 108.69 ± 30.65; $P < 0.01$) (Fig. 2b). Meanwhile, the binding of [^{99m}Tc]Tc-NB4 to HT-29 cells was significantly inhibited by the addition of an excess cold NB4 (from $73{,}412.20 \pm 5689.99$ to 1337.61 ± 43.13; $P < 0.01$). Fluorescent staining revealed that NB4 accumulated on the cell membrane of HT-29 cells where EpCAM was expressed (Fig. 2c), whereas HL-60 cells could hardly be stained with NB4. These results suggest that NB4 has a great specificity for EpCAM in vitro.

Fig. 3 **a** Representative static SPECT/CT images of the HT-29 tumor-bearing mice (EpCAM positive, red dashed circle) administered with 18 MBq [^{99m}Tc]Tc-NB4. K, T, and B indicate kidney, tumor, and bladder, respectively. **b** Biodistribution of [^{99m}Tc]Tc-NB4 in HT-29 tumor-bearing mice. **c** Tumor/muscle ratios of [^{99m}Tc]Tc-NB4 in HT-29 tumor-bearing nude mice. **d** Blocking study of [^{99m}Tc]Tc-NB4 biodistribution in HT-29 tumor-bearing nude mice at 2 h after injection. The blocking group was co-injected with an excess cold NB4 (1 mg) as a blocking agent. ns, $P > 0.05$
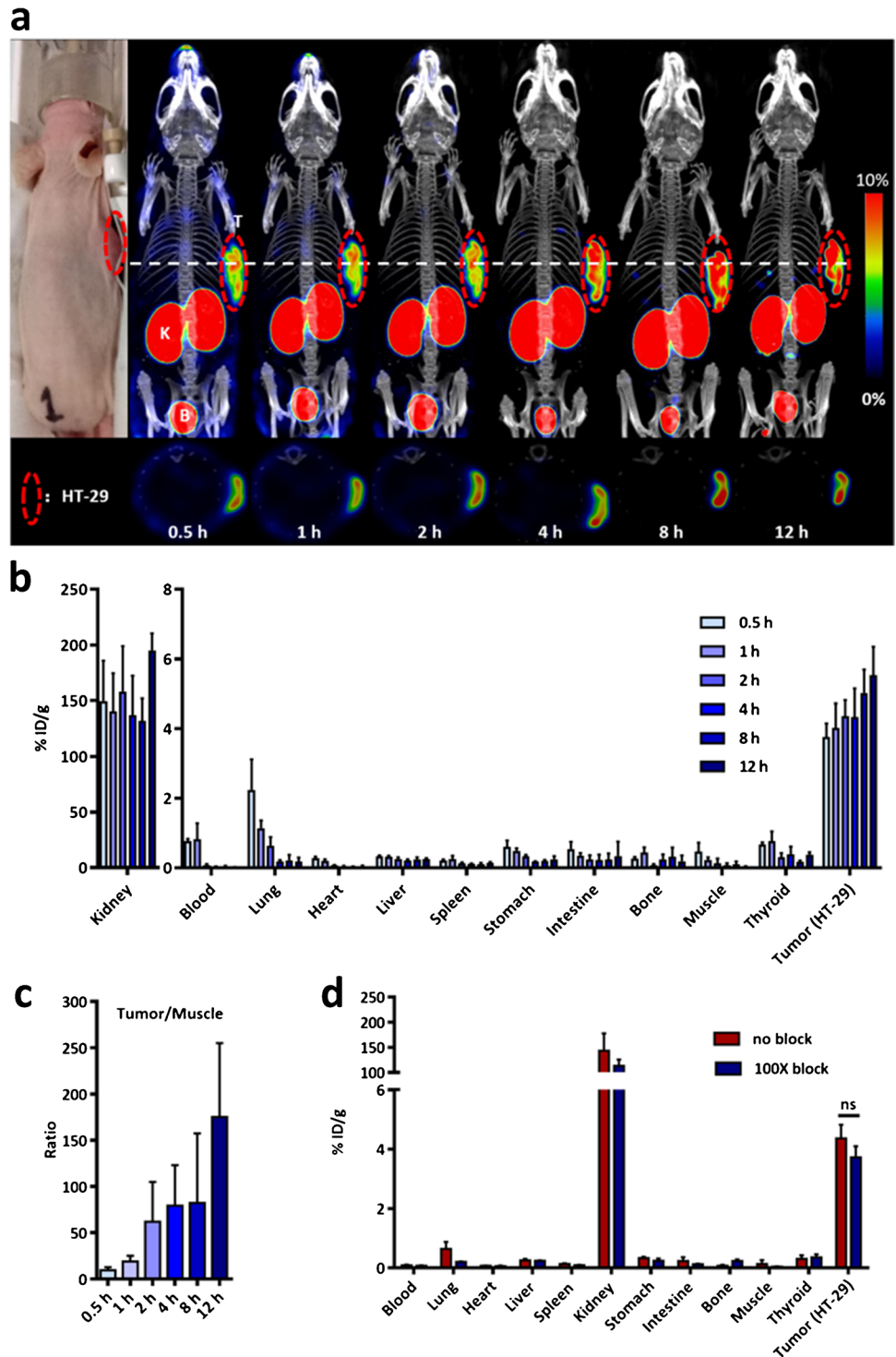
SPECT/CT imaging

The SPECT/CT imaging was performed in mice with HT-29 tumor xenografts at 30 min, 1 h, 2 h, 4 h, 8 h, and 12 h after the injection of [^{99m}Tc]Tc-NB4, and the images showed a time-dependent tumor accumulation of radiotracer (Fig. 3a). At 2 h p.i., the uptake of [^{99m}Tc]Tc-NB4 in other organs was reduced to a lower level due to the rapid clearance of nanobody from the body, while the uptake of [^{99m}Tc]Tc-NB4 in kidneys and bladder was higher because nanobody is mainly metabolized by the urinary system.

Ex vivo biodistribution

In order to evaluate the distribution of [^{99m}Tc]Tc-NB4 in vivo, animals were sacrificed at designated time points, and the results were summarized in Fig. 3b and Table S1. The increase of tumor uptake over time in imaging experiments was basically consistent with that in biodistribution. The HT-29 tumor uptake values of [^{99m}Tc]Tc-NB4 were 3.77 ± 0.39, 4.02 ± 0.70, 4.36 ± 0.46, 4.33 ± 0.82, 5.02 ± 0.67, and 5.53 ± 0.82 %ID/g at 30 min, 1 h, 2 h, 4 h, 8 h, and 12 h p.i., showing an upward trend over time. Nevertheless, due to the rapid clearance of the unbound probe in vivo, the uptake values of [^{99m}Tc]Tc-NB4 in blood and muscle tissue tended to decrease over time. Taking muscle tissue as an example, the uptake values were 0.47 ± 0.25, 0.22 ± 0.08, 0.13 ± 0.14, 0.08 ± 0.06, 0.10 ± 0.08, and 0.03 ± 0.01 %ID/g at 30 min, 1 h, 2 h, 4 h, 8 h, and 12 h p.i. Accordingly, the values of tumor/muscle changed from 9.38 ± 3.38 at 30 min p.i. to 175.30 ± 79.66 at 12 h p.i. (Fig. 3c). In other words, the tumor uptake of [^{99m}Tc]Tc-NB4 was significantly higher than that in the blood and most other normal organs at almost all time points examined. The uptake value of kidneys was highest because [^{99m}Tc]Tc-NB4 is primarily excreted by the kidneys.

In the blocking study (Fig. 3d), mice were co-injected with [^{99m}Tc]Tc-NB4 and cold NB4 which was more than 100 times the dose of [^{99m}Tc]Tc-NB4. The tumor uptake (3.73 ± 0.37 %ID/g) in the blocking group was not significantly different from the [^{99m}Tc]Tc-NB4 group. All organs showed similar uptake levels in two groups. Due to the large abundance of EpCAM expressed on the cell membrane [13], co-injection of 100-fold excess cold NB4 could not effectively block the uptake of [^{99m}Tc]Tc-NB4 in tumors.

[^{99m}Tc]Tc-NB4 SPECT/CT and [^{18}F]FDG PET/CT in the bilateral tumor model

In order to validate the EpCAM-targeted specificity of [^{99m}Tc]Tc-NB4 imaging, we established the bilateral tumor-bearing mouse model according to the timeline in Fig. 4a to keep the same size of tumors. We first performed the biodistribution experiment to compare tumor uptake on both sides, while the uptake in EpCAM-positive tumors was much higher than that in EpCAM-negative tumors (HT-29: 5.73 ± 1.45 %ID/g vs. HL-60: 0.18 ± 0.17 %ID/g, $P < 0.01$) (Fig. 4b). For the [^{99m}Tc]Tc-NB4 SPECT/CT imaging, the HT-29 tumors were clearly visible, whereas there was almost no radioactive signal in HL-60 tumors (Fig. 4c), which was consistent with the biodistribution result. For the [^{18}F]FDG PET/CT imaging, both HT-29 and HL-60 tumors could be clearly visualized (SUV 2.95 vs. 2.44) (Fig. 4c), which could not distinguish EpCAM-positive and EpCAM-negative tumors. As the immunofluorescence staining results (Fig. 4d), the HT-29 tumor tissues showed high Dylight-NB4 immunoreactivity. In contrast, HL-60 tumor tissues were hardly stained with Dylight-NB4.

[^{99m}Tc]Tc-NB4 SPECT/CT in a lymphatic metastasis model

In order to verify the sensitivity of the probe, we established a lymphatic metastasis model by footpad inoculation of HT-29-Luc tumor cells into the left front and hind footpads of mice. When the in vivo BLI showed HT-29 tumor metastases in the left axillary lymph nodes and popliteal lymph nodes of mice on day 21, the [^{99m}Tc]Tc-NB4 SPECT/CT imaging was carried out in this model 2 days later (Fig. 5a). As shown in Fig. 5b, although the lymph nodes were very small, they were also clearly visualized, and the probe uptake in tumor-draining lymph nodes was markedly higher compared to that of the control contralateral normal lymph nodes.

In order to further verify the probe aggregation in the lymph nodes, we used 1% Evans Blue by footpad injection to locate lymph nodes, then surgically removed axillary and popliteal lymph nodes and placed them next to the mouse to re-image. The radioactive signals of the original lymph nodes disappeared (Fig. 5c), which proved that the location of the probe aggregation was indeed the lymph node area.

Tumor-draining lymph nodes and normal lymph nodes were collected after SPECT imaging and subjected to H&E staining and immunofluorescence staining. Compared with the normal lymph nodes, the tumor-infiltrating lymph nodes showed obvious cancer nests, mitotic figures, and atypia (Fig. 6a), as well as the higher Dylight-NB4 immunoreactivity (Fig. 6b).

Discussion

EpCAM plays a normal physiological function in normal tissues as a functional molecule, and its overexpression in tumor tissues makes it an excellent diagnostic and therapeutic target. Previous studies have shown that the expression

Fig. 4 **a** Schedule of [^{18}F]FDG PET/CT and [^{99m}Tc]Tc-NB4 SPECT/CT imaging. **b** Biodistribution of [^{99m}Tc]Tc-NB4 in HT-29/HL-60 bilateral tumor-bearing mice at 2 h after injection. **, $P < 0.01$. **c** Representative images of [^{99m}Tc]Tc-NB4 SPECT/CT and [^{18}F]FDG PET/CT in the HT-29/HL-60 bilateral tumor-bearing mice. **d** Immunofluorescence staining of EpCAM in HT-29 and HL-60 tumor tissues
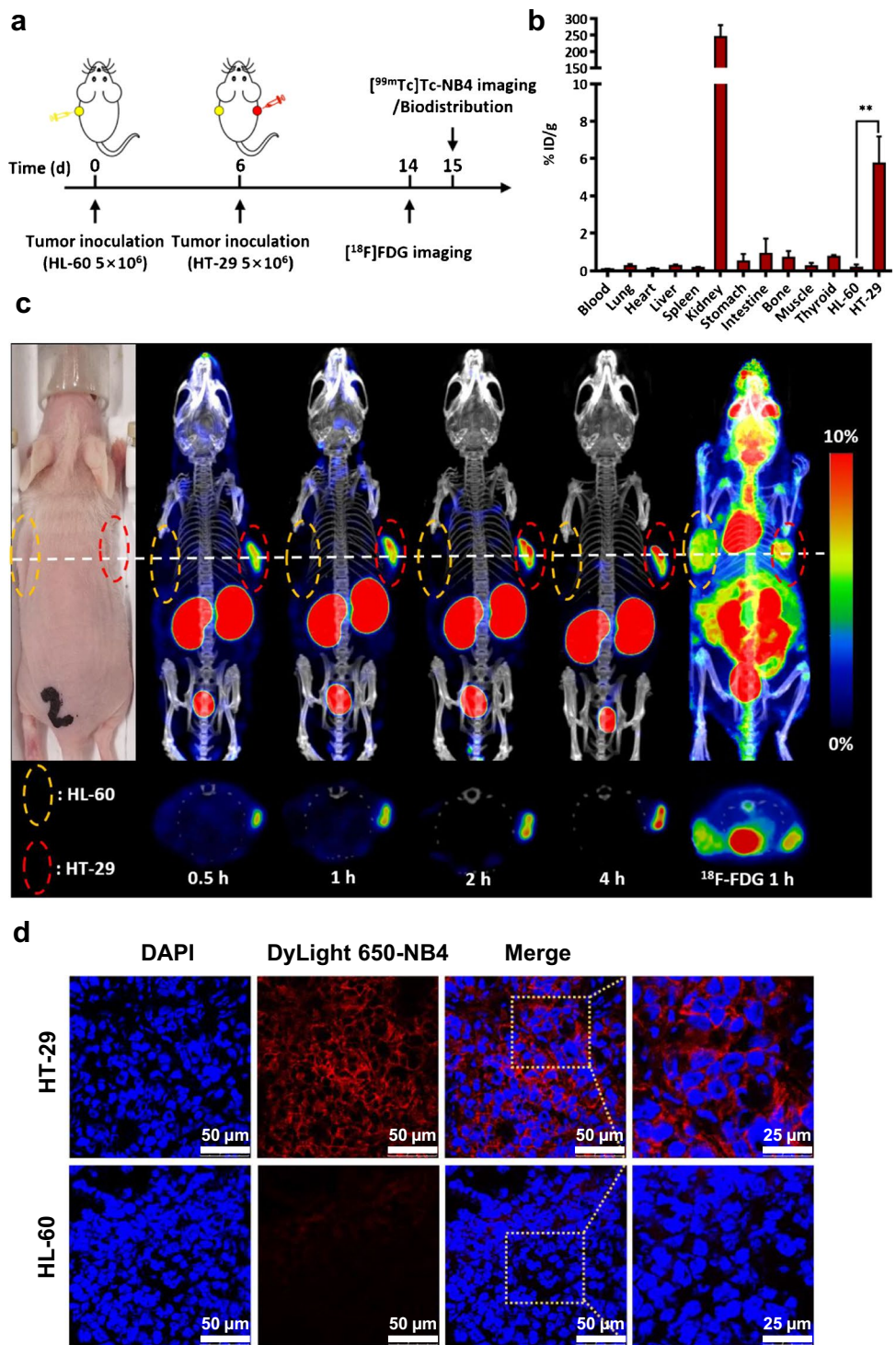
level of EpCAM in breast cancer, liver cancer, and pancreatic cancer is associated with poor prognosis, whereas the overexpression of EpCAM molecule in thyroid cancer and renal cancer has a good prognosis [23]. EpCAM can inhibit or promote tumor growth in different tumor types, thereby the detection of EpCAM can provide a guidance to make the treatment plan for cancer patients. In this study, we

developed a new radiolabeled EpCAM-targeted nanobody [^{99m}Tc]Tc-NB4, which can be used as a broad-spectrum tumor imaging agent for the diagnosis, staging, and prognosis. In the meanwhile, the development of EpCAM-specific antibodies in recent years offers the possibility of EpCAM-targeted immunotherapy. However, due to the tumor heterogeneity and different EpCAM expression levels of patients,

Fig. 5 **a** Timeline illustration of tumor inoculation, BLI optical imaging, and [^{99m}Tc]Tc-NB4 SPECT/CT imaging. **b** BLI of the HT-29-Luc lymph node (LN) metastasis model on day 21, and representative [^{99m}Tc]Tc-NB4 SPECT/CT images in this model at 3 h p.i. Coronal 2D images of axillary and popliteal LNs are shown. Yellow arrows refer to lymph node metastases. **c** Re-imaging of surgically removed LNs to verify the [^{99m}Tc]Tc-NB4 accumulation in tumor-draining lymph nodes
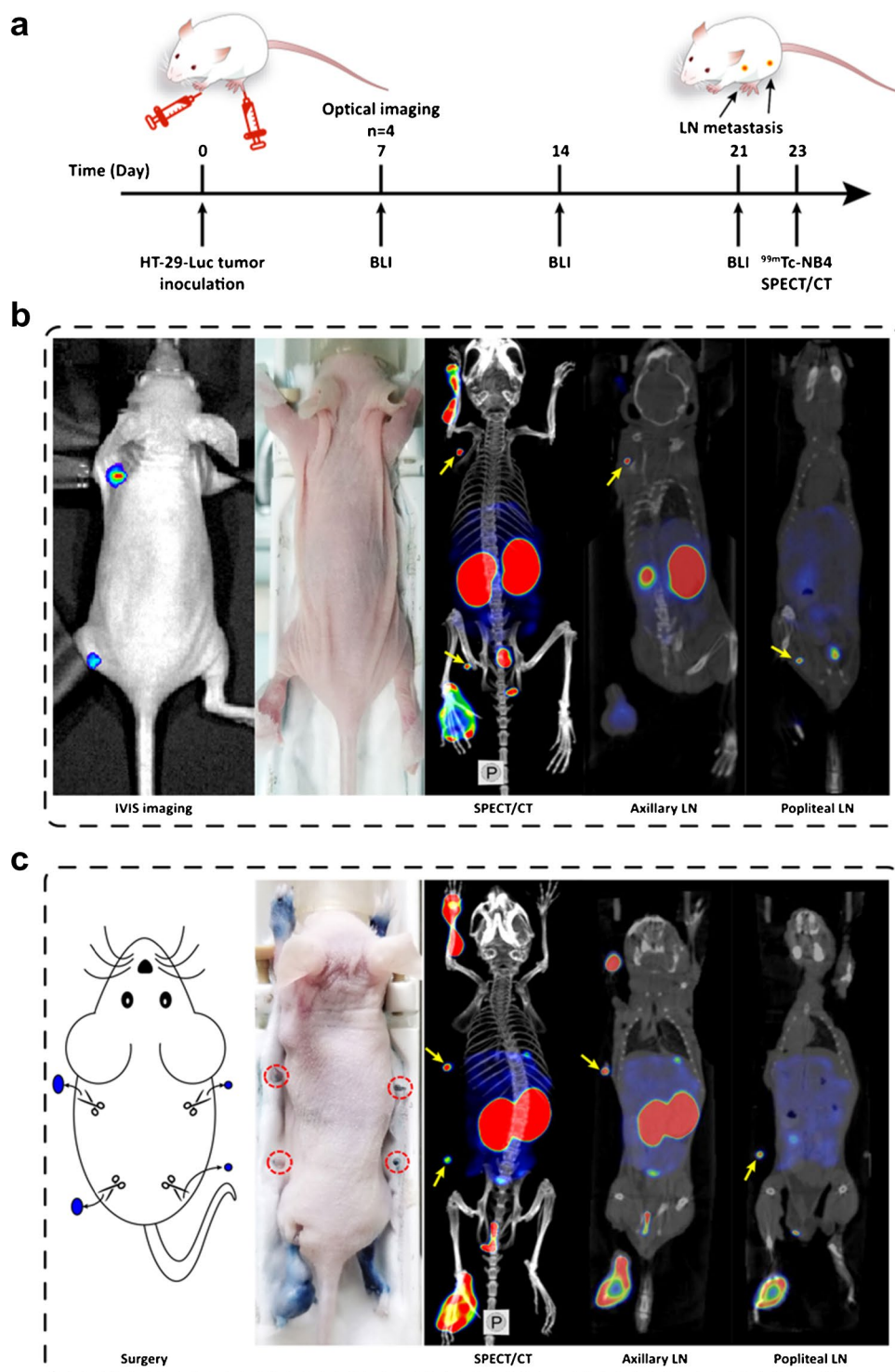

not all patients can benefit from immunotherapy [24]. By monitoring the expression level of EpCAM in vivo during immunotherapy, [^{99m}Tc]Tc-NB4 SPECT/CT can be used to guide the individualized treatment in the clinic.

In this study, we used the site-specific radiolabeling strategy to prepare the nanobody probe [^{99m}Tc]Tc-NB4. The stable imaging quality up to 12 h indirectly demonstrates the high stability of the [[^{99m}Tc]Tc-HYNIC(TPPTS)(Tricine)] site-specific radiolabeling system in vivo (Fig. 3a. This strategy is very important for reducing nonspecific radioactive signals in organs other than tumors. The rapid clearance of [^{99m}Tc]Tc-NB4 from blood and other organs ensures the high tumor-to-background ratio necessary for an imaging agent. We did not choose a radiolabeled monoclonal

Fig. 6 H&E staining (**a**) and Immunofluorescence staining (**b**) of tumor-draining lymph nodes and normal lymph nodes
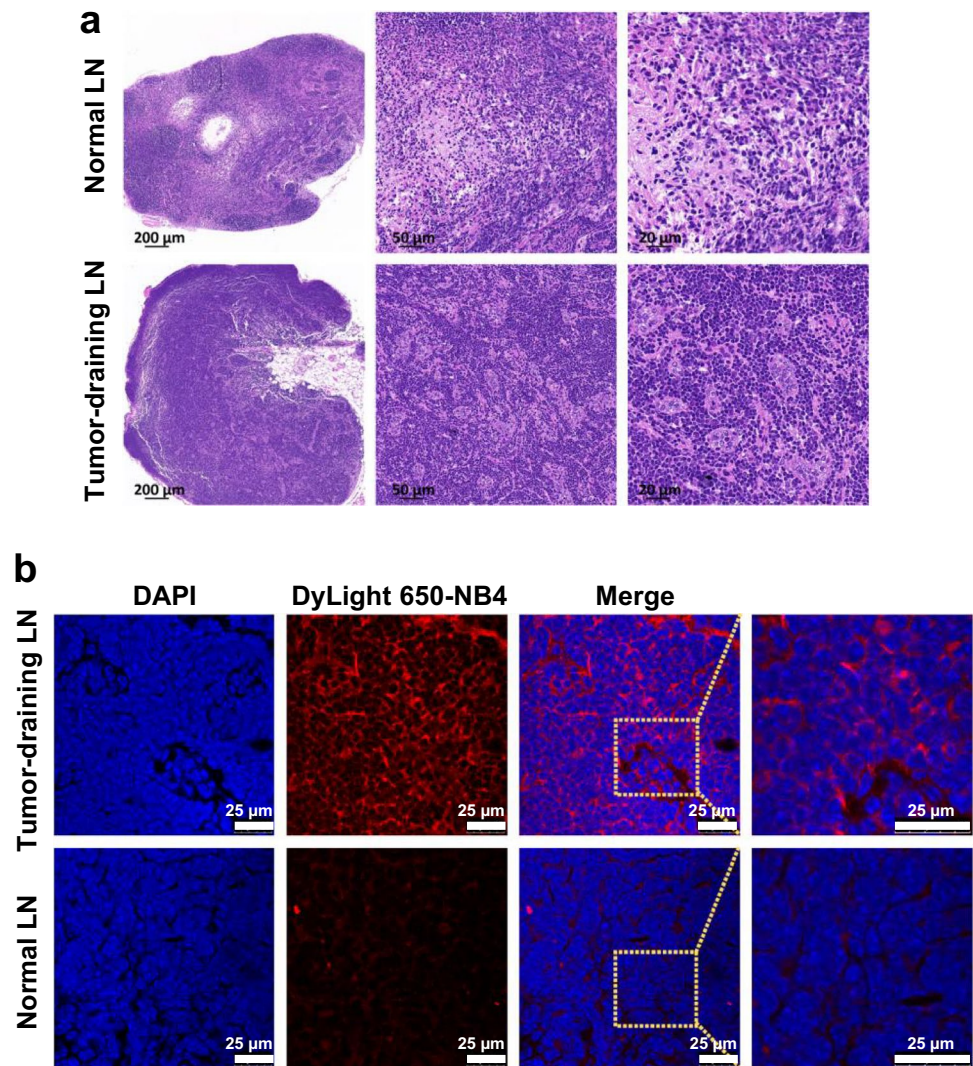
antibody for nuclear medicine imaging because its imaging time is 3–7 days p.i., which is not convenient for clinical application. For the clinical application of nanobody probes, the biggest advantage is that it can be used for same-day imaging, and the tumor is clear enough at 2 h p.i. (Fig. 3a). [^{99m}Tc]Tc-NB4's rapid distribution and high signal-to-noise ratio in vivo (Fig. 3b, c) ensure the need for fast noninvasive diagnostic imaging, which is a great advantage for clinical application. Our radioactive probe can be used for further confirmation when a clinically routine CT/MRI examination produces a suspected abnormality.

As the most widely used nuclear medicine imaging agent, [^{18}F]FDG is used to detect tumors in clinical, but it is not a specific imaging agent and cannot judge the expression of EpCAM in tumors (Fig. 4c). As an EpCAM-targeted tumor imaging agent, [^{99m}Tc]Tc-NB4 showed the high EpCAM specificity at protein and cellular levels. In animal models, [^{99m}Tc]Tc-NB4 SPECT/CT revealed the

rapid accumulation and relatively high uptake in subcutaneous EpCAM-positive HT-29 tumors, while it was unable to image EpCAM-negative HL-60 tumors (Fig. 4c). This further showed the high specificity of this probe. Current preclinical studies have shown that for HT-29 and some other common tumors, the expression of EpCAM on the surface of each tumor cell exceeds 2×10^6 receptors, which is a receptor with high abundance [13, 25

The HT-29 tumor uptake of [^{99m}Tc]Tc-NB4 increased with time, while the uptake in other organs except for the kidneys rapidly decreased (Fig. 3). [^{99m}Tc]Tc-NB4 had a high renal uptake value in biodistribution and SPECT/CT imaging. If [^{99m}Tc]Tc-NB4 would be used in clinical imaging in the future, the radiation damage to kidneys could be eliminated by pre-injection of renal protective agents (such as Gelofusine and lysine) [26]. The results of SPECT imaging and biodistribution experiments showed that [^{99m}Tc]Tc-NB4 retained a relatively high tumor uptake for

a relatively long time (Fig. 3). In vitro cell internalization experiment showed that the internalization ratio of [99mTc]Tc-NB4 was rather low, and this probe was mostly bound to EpCAM receptors on the cell membrane (Fig S3). These results reveal that our nanobody has a good binding ability to the EpCAM receptor and has less dissociation after binding. The uptake characteristics of [99mTc]Tc-NB4 in tumors merits future radioimmunotherapy research by labeling NB4 nanobody with therapeutic nuclides. The high cumulative dose of radioactivity in tumors has a great impact on the treatment. We will continue to explore the imaging and biodistribution of radiolabeled NB4 after 12 h in subsequent experiments.

Clinical staging and prognosis were evaluated by lymph node metastasis. SPECT/CT imaging with [99mTc]Tc-NB4 could accurately locate small lymph node metastasis tumors (< 5 mm in diameter) (Fig. 5b). The clear imaging of tumor-draining lymph nodes showed a high sensitivity of [99mTc]Tc-NB4, which makes the early diagnosis of tumor and tumor metastasis possible. [99mTc]Tc-NB4 could accurately distinguish tumor lymph nodes from normal lymph nodes in animal studies (Fig. 5c), which showed a potential to help physicians to stage patients and further formulate surgery and treatment strategies.

The resolution and sensitivity of clinical SPECT/CT imaging were relatively lower than PET/CT imaging, and 99mTc drugs were relatively limited in technology development, so the overall development of 99mTc SPECT/CT for tumors was relatively slow [27]. However, in the past 20 years, on the one hand, the progress of technetium chemistry has promoted the development of new 99mTc radiopharmaceuticals; on the other hand, the development of detector technology and the progress of reconstruction algorithm in imaging equipment make the spatial resolution of SPECT closer to that of PET, and the sensitivity does not decrease [28]. These signs of progress bring new development opportunities for SPECT/CT technology. Furthermore, the optimal imaging time of nanobody probes is also perfectly consistent with the half-life of 99mTc, thus [99mTc]Tc-NB4 SPECT/CT has a great potential for clinical translation.

Conclusions

The present study developed and evaluated a new nanobody-based molecular probe [99mTc]Tc-NB4 targeting EpCAM for SPECT/CT imaging. [99mTc]Tc-NB4 revealed the high specificity and sensitivity and could clearly image EpCAM-positive tumors and lymph node metastasis in vivo. This probe can be used as a broad-spectrum probe for the diagnosis, staging, and prognosis of cancer patients. Furthermore, it can be used to guide the individualized treatment of EpCAM-targeted drugs. [99mTc]Tc-NB4 SPECT/CT has a great potential for clinical translation.

Declarations

Ethical approval All applicable international, national, and/or institutional guidelines for the care and use of animals were followed. This article does not contain any studies with human participants performed by any of the authors.

Conflict of interest The authors declare no competing interests.

References

1. Baeuerle P, Gires O. EpCAM (CD326) finding its role in cancer. Br J Cancer. 2007;96:417–23.
2. Litvinov S, Balzar M, Winter M, Bakker H, Briaire-de Bruijn I, Prins F, et al. Epithelial cell adhesion molecule (Ep-CAM) modulates cell-cell interactions mediated by classic cadherins. J Cell Biol. 1997;139:1337–48.
3. Went P, Lugli A, Meier S, Bundi M, Mirlacher M, Sauter G, et al. Frequent EpCam protein expression in human carcinomas. Hum Pathol. 2004;35:122–8.
4. Went P, Vasei M, Bubendorf L, Terracciano L, Tornillo L, Riede U, et al. Frequent high-level expression of the immunotherapeutic target Ep-CAM in colon, stomach, prostate and lung cancers. Br J Cancer. 2006;94:128–35.
5. Spizzo G, Went P, Dirnhofer S, Obrist P, Moch H, Baeuerle P, et al. Overexpression of epithelial cell adhesion molecule (Ep-CAM) is an independent prognostic marker for reduced survival of patients with epithelial ovarian cancer. Gynecol Oncol. 2006;103:483–8.
6. Spizzo G, Went P, Dirnhofer S, Obrist P, Simon R, Spichtin H, et al. High Ep-CAM expression is associated with poor prognosis in node-positive breast cancer. Breast Cancer Res Treat. 2004;86:207–13.
7. Riethmüller G, Holz E, Schlimok G, Schmiegel W, Raab R, Höffken K, et al. Monoclonal antibody therapy for resected Dukes' C colorectal cancer: seven-year outcome of a multicenter randomized trial. J Clin Oncol. 1998;16:1788–94.
8. Riethmüller G, Schneider-Gädicke E, Schlimok G, Schmiegel W, Raab R, Höffken K, et al. Randomised trial of monoclonal antibody for adjuvant therapy of resected Dukes' C colorectal carcinoma. German Cancer Aid 17–1A Study Group. Lancet. 1994;343:1177–83.
9. Punt C, Nagy A, Douillard J, Figer A, Skovsgaard T, Monson J, et al. Edrecolomab alone or in combination with fluorouracil and folinic acid in the adjuvant treatment of stage III colon cancer: a randomised study. Lancet. 2002;360:671–7.
10. Massoud T, Gambhir S. Molecular imaging in living subjects: seeing fundamental biological processes in a new light. Genes Dev. 2003;17:545–80.

11. Eder M, Knackmuss S, Le Gall F, Reusch U, Rybin V, Little M, et al. 68Ga-labelled recombinant antibody variants for immuno-PET imaging of solid tumours. Eur J Nucl Med Mol Imaging. 2010;37:1397–407.

12. Hall M, Pinkston K, Wilganowski N, Robinson H, Ghosh P, Azhdarinia A, et al. Comparison of mAbs targeting epithelial cell adhesion molecule for the detection of prostate cancer lymph node metastases with multimodal contrast agents: quantitative small-animal PET/CT and NIRF. J Nucl Med. 2012;53:1427–37.

13. Warnders F, Waaijer S, Pool M, Lub-de Hooge M, Friedrich M, Terwisscha van Scheltinga A, et al. Biodistribution and PET imaging of labeled bispecific T cell-engaging antibody targeting EpCAM. J Nucl Med. 2016;57:812–7.

14. Hamers-Casterman C, Atarhouch T, Muyldermans S, Robinson G, Hamers C, Songa E, et al. Naturally occurring antibodies devoid of light chains. Nature. 1993;363:446–8.

15. Steeland S, Vandenbroucke R, Libert C. Nanobodies as therapeutics: big opportunities for small antibodies. Drug Discov Today. 2016;21:1076–113.

16. Rashidian M, Keliher E, Dougan M, Juras P, Cavallari M, Wojtkiewicz G, et al. The use of F-2-fluorodeoxyglucose (FDG) to label antibody fragments for immuno-PET of pancreatic cancer. ACS Cent Sci. 2015;1:142–7.

17. Guimaraes CP, Witte MD, Theile CS, Bozkurt G, Kundrat L, Blom AEM, et al. Site-specific C-terminal and internal loop labeling of proteins using sortase-mediated reactions. Nat Protoc. 2013;8:1787–99. https://doi.org/10.1038/nprot.2013.101.

18. Theile C, Witte M, Blom A, Kundrat L, Ploegh H, Guimaraes C. Site-specific N-terminal labeling of proteins using sortase-mediated reactions. Nat Protoc. 2013;8:1800–7.

19. Dong C, Yang S, Shi J, Zhao H, Zhong L, Liu Z, et al. SPECT/NIRF dual modality imaging for detection of intraperitoneal colon tumor with an avidin/biotin pretargeting system. Sci Rep. 2016;6:18905.

20. Zhang CR, Yu XH, Gao LQ, Zhao Y, Lai JH, Lu DH, et al. Non-invasive imaging of CD206-positive M2 macrophages as an early biomarker for post-chemotherapy tumor relapse and lymph node metastasis. Theranostics. 2017;7:4276–88. https://doi.org/10.7150/thno.20999.

21. Zhang C, Gao L, Cai Y, Liu H, Gao D, Lai J, et al. Inhibition of tumor growth and metastasis by photoimmunotherapy targeting tumor-associated macrophage in a sorafenib-resistant tumor model. Biomaterials. 2016;84:1–12.

22. Li L, Wu Y, Wang Z, Jia B, Hu Z, Dong C, et al. SPECT/CT imaging of the novel HER2-targeted peptide probe Tc-HYNIC-H6F in breast cancer mouse models. J Nucl Med. 2017;58:821–6.

23. Mashhadi SMY, Kazemimanesh M, Arashkia A, Azadmanesh K, Meshkat Z, Golichenari B, et al. Shedding light on the EpCAM: an overview. J Cell Physiol. 2019;234:12569–80. https://doi.org/10.1002/jcp.28132.

24. Macdonald J, Henri J, Roy K, Hays E, Bauer M, Veedu RN, et al. EpCAM immunotherapy versus specific targeted delivery of drugs. Cancers. 2018. https://doi.org/103390/cancers10010019.

25. Thurber GM, Weissleder R. Quantitating antibody uptake in vivo: conditional dependence on antigen expression levels. Mol Imag Biol. 2011;13:623–32. https://doi.org/10.1007/s11307-010-0397-7.

26. Chatalic KLS, Veldhoven-Zweistra J, Bolkestein M, Hoeben S, Koning GA, Boerman OC, et al. A novel in-111-labeled anti-prostate-specific membrane antigen nanobody for targeted SPECT/CT imaging of prostate cancer. J Nucl Med. 2015;56:1094–9. https://doi.org/10.2967/jnumed.115.156729.

27. Boschi A, Uccelli L, Martini P. A picture of modern Tc-99m radiopharmaceuticals: production, chemistry, and applications in molecular imaging. Appl Sci-Basel. 2019;9:2526. https://doi.org/10.3390/app9122526.

28. Van den Wyngaert T, Elvas F, De Schepper S, Kennedy JA, Israel O. SPECT/CT: standing on the shoulders of giants, it is time to reach for the sky! J Nucl Med. 2020;61:1284–91. https://doi.org/10.2967/jnumed.119.236943.